Acta Cryst. (1994). B**50**, 135–141

Relationship Between the Structures of Ferroelectric $Pb_5Cr_3F_{19}$ and Antiferroelectric $Pb_5Al_3F_{19}$ at 295 K and the Phase III–Phase IV Transition in $Pb_5Al_3F_{19}$ on Cooling to about 110 K

BY V. ANDRIAMAMPIANINA, P. GRAVEREAU AND J. RAVEZ

Laboratoire de Chimie du Solide du CNRS, Université Bordeaux I, F-33405 Talence CEDEX, France

AND S. C. ABRAHAMS

Physics Department, Southern Oregon State College, Ashland, OR 97520, USA

(*Received* 17 *May* 1993; *accepted* 29 *September* 1993)

Abstract

Antiferroelectric phase III of lead aluminium fluoride, $Pb_5Al_3F_{19}$, $M_r = 1477.9$, tetragonal space group $P4/n$. At $T = 295$ K, $a = 20.1738$ (4) and $c = 7.2205$ (1) Å, $V = 2939$ (1) Å^3, $Z = 8$, $D_m = 6.66$ (5), $D_x = 6.681$ Mg m^{-3}. For λ(Mo $K\alpha$) = 0.71069 Å, $\mu = 58.0$ mm^{-1}, $F(000) = 4960$. The structure was determined from 18502 (1276 independent) $F_m^2 \geq 3\sigma(F_m^2)$ with $(\sin\theta)/\lambda \leq 0.703$ Å^{-1}. Least-squares refinement on wF_m^2 resulted in $R(F_m) = 0.0579$ with $R_{int}(F_m) = 0.048$. $Pb_5Al_3F_{19}$ undergoes a first-order phase transition from antiferroelectric to ferroelectric at about 110 K, with a wide thermal hysteresis. Transformation of the atomic coordinates of ferroelectric $Pb_5Cr_3F_{19}$ previously measured at 295 K and comparison with those of antiferroelectric $Pb_5Al_3F_{19}$ at 295 K reveal differences between related atomic positions that range from 0.10 to 1.56 Å. The origin of the first-order transition from the antiferroelectric phase III to ferroelectric phase IV in $Pb_5Al_3F_{19}$ is shown to be associated with the orientational change from an eclipsed arrangement of AlF_6 octahedra along the inversion and rotation-tetrad axes in phase III to a staggered arrangement along the rotation-tetrad axes in phase IV.

Introduction

$Pb_5Cr_3F_{19}$ undergoes a first-order phase transition at 555 K (Arquis-Canouet, Ravez & Abrahams, 1986) that was later shown to be from the paraelectric to the ferroelectric phase, on cooling (Ravez, Andriamampianina, Simon, Grannec & Abrahams, 1991). The displacement magnitudes of the symmetry-independent Cr atoms from the centers of their fluorine octahedra allow a transition temperature of 630 (30) K to be predicted (Abrahams, Kurtz & Jamieson, 1968), in satisfactory agreement with experiment (Abrahams, Albertsson, Svensson & Ravez, 1990). $Pb_5Cr_3F_{19}$ forms a continuous series of ferroelectric solid solutions with $Pb_5Al_3F_{19}$; the transition temperatures of the resulting materials, as measured on heating, decrease smoothly from 555 to 280 K with increasing $Pb_5Al_3F_{19}$ component (Ravez, Simon, Andriamampianina, Grannec, Hagenmuller & Abrahams, 1990; Andriamampianina, Ravez, Simon & Abrahams, 1991). The phase diagram of the $Pb_5(Cr_{1-x}Al_x)_3F_{19}$ system has been determined, under both heating and cooling conditions, by Ravez, Andriamampianina, Simon, Rabardel, Ihringer & Abrahams (1994).

The low temperature of the phase transition and associated wide thermal hysteresis in $Pb_5Al_3F_{19}$, together with the closely related $Pb_5Cr_3F_{19}$ structure, led to the present investigation of the $Pb_5Al_3F_{19}$ atomic arrangement at room temperature in the possibility that light might thereby be cast upon the structural changes characterizing the transition from the ferroelectric to the antiferroelectric phase. Room-temperature phase III of $Pb_5Al_3F_{19}$ is referred to as antiferroelectric, rather than as paraelectric, since phase I is the prototypic paraelectric phase stable above 345 K (Ravez *et al.*, 1994) and point group $4/m$ for phase III is not a supergroup of $4mm$ for ferroelastic phase IV, the stable phase at lower temperatures. The second-order transition from phase I (point group $4/m$) to phase II (point group $2/m$) is accompanied by the formation of domains that disappear sharply at the first-order transition from phase II to phase III. The monoclinic distortion in phase II is small, with $a \simeq b$ and maximum departure by the angle β of 0.41 (2)° from 90°. The domains in phase II result from the twin law originating in the replacement of fourfold by twofold axes at the higher temperature phase I–phase II transition. Restoration of the fourfold axes on cooling further from phase II to phase III necessarily eliminates all remaining domains at this phase transition, as confirmed by careful optical examination. Etching techniques for revealing the unlikely possibility of domain boundaries were inapplicable. Peritectic decomposition

©1994 International Union of Crystallography
Printed in Great Britain – all rights reserved

begins above 925 K, precluding thermal etching; the only solvents capable of chemical etching lead to hydrolysis. The lattice temperature dependence of $Pb_5Al_3F_{19}$ through all three phase transitions has been given in a paper dedicated to Professor E. F. Bertaut on the occasion of his eightieth birthday (Ihringer, Ravez & Abrahams, 1993).

Crystal growth

The most successful of several crystal-growth methods investigated depend upon a controlled slow cooling of the molten phase. Initial ingredients consisted of a mixture of PbF_2 and AlF_3, with expected purities greater than 99.9%, in the ratio 1.66:1. This mix was placed within a gold tube in a dry box, degassed at 423 K for 4 h and sealed under dry N_2. Following heating to 993 K, maintaining this temperature for 24 h and then cooling to 823 K at a rate of 10 K h^{-1}, the furnace was allowed to return to room temperature by natural cooling. The gold tube was typically found to contain many transparent colorless single crystals, generally in the form of rectangular prisms elongated along the c axis. Average crystal dimensions are about 0.1 × 0.1 × 0.5 mm.

Structural measurement

All integrated intensities within the volume of reciprocal space bounded by $h - 28 \rightarrow 28$, $k - 28 \rightarrow 28$, l $0 \rightarrow 10$ and $0 \le \theta \le 30°$ were measured at $T =$ 295 K using an Enraf–Nonius CAD-4 diffractometer with a prismatic $Pb_5Al_3F_{19}$ crystal of good optical quality that exhibited sharp extinction and that had the dimensions 0.115 × 0.134 × 0.120 mm. Mo $K\alpha$ radiation diffracted by a graphite monochromator was used with ω–2θ scans over an angular range 0.60 + 0.35°tanθ. Reflection halfwidths ranged from 0.15 to 0.30° θ. Three standard reflections were measured following each 200th reflection. The total exposure time was 360 h. No systematic variation was detected in the intensity of the standards as a function of exposure. Transmission factors obtained by integration from the crystal shape ranged from 0.0136 to 0.0488. Weights, calculated only from counting statistics, were taken as $1/\sigma^2(F_m)$.

The diffraction symmetry of $Pb_5Al_3F_{19}$ phase III is $4/m$. The only systematically absent reflections are $hk0$ with $h + k = 2n + 1$, hence the most likely space group is $P4/n$. The primitive unit cell of phase III is rotated 45° about c with respect to the orientation of phases I, II or IV (Ravez *et al.*, 1994). The I centering of these three phases results in pseudo F centering for phase III, as may be noted in the intensity condition that $I(hkl)$ with $h + k$, $k + l$, $h + l = 2n$ is generally much stronger than are reflections with odd index-pair values, see Supplementary Publication No. SUP 71567.* Structure refinement of phase III was initiated on the assumption that the Pb-atom distribution would be similar to that in ferroelectric $Pb_5Cr_3F_{19}$ (Abrahams *et al.*, 1990). Successive electron-density difference maps revealed the location of the five independent Al and 22 independent F atoms. Least-squares refinement with the *SHELX* (Sheldrick, 1976) program, based on isotropic thermal vibrations, resulted in $R = 0.077$, $wR = 0.087$. Inclusion of individual B_{iso} parameters for all Al and F atoms led to a wide range of values, some of which were without physical significance. Fitting anisotropic displacement coefficients to each Pb atom, but with a common variable B_{iso} parameter for all Al atoms and another for all F atoms, it was found necessary to set the z coordinates of F1 and F2 in Wyckoff position 2(c) to the fixed values of 0 and $\frac{1}{2}$ respectively in order to avoid abnormal Al—F distances resulting from the refinement; however, omitting these atoms from the structure-factor calculations led to the appearance of ~ 17 e Å^{-3} maxima in the ensuing difference maps at about $\frac{1}{4}$, $\frac{1}{4}$, z with $z = 0$ and $\frac{1}{2}$. The heights of the other F atoms in earlier difference maps ranged from 10.2 to 19.5 e Å^{-3}. The final atomic coordinates presented in Table 1 correspond to $R = 0.0579$, $wR = 0.0648$ and $S = 1.837$ for a total of 112 variables, based on the empirical correction for extinction given by $F_{corr} = F_m[1 - 10^{-4} gF_m^2/(\sin\theta)]$ with $g = 8(1) \times 10^{-5}$. Oscillatory behavior in refinement led slowly to the final minimum in wR with no value of Δ/σ exceeding 0.3. The largest residual in the corresponding final difference map was a feature of 6 e Å^{-3} magnitude located about 1 Å from Pb5 at $z \simeq 0.237$.

$Pb_5Al_3F_{19}$ antiferroelectric phase III

The structure of antiferroelectric phase III generally resembles that of ferroelectric phase IV. Both consist of infinite corner-sharing chains of AlF_6 octahedra, individual AlF_6 octahedra, individual F^- ions and Pb^{2+} ions occupying the polyhedra formed by the F^- ions. As may be seen in Fig. 1, all octahedra in the infinite chains of phase III have the same orientation leading to an eclipsed configuration along the c axis. The doubling of the unit cell volume in this phase, with respect to phase IV, results from the formation of two different sets of corner-sharing chains, one containing symmetry-independent Al1 F_6 and Al2 F_6 octahedra, and the other consisting

* Lists of structure factors and anisotropic displacement coefficients for the lead atoms have been deposited with the British Library Document Supply Centre as Supplementary Publication No. SUP 71567 (7 pp.). Copies may be obtained through The Technical Editor, International Union of Crystallography, 5 Abbey Square, Chester CH1 2HU, England. [CIF reference: ST0617]

Table 1. *Atomic coordinates* ($\times 10^4$) *and equivalent* (Pb) *or isotropic* (Al, F) *displacement coefficients* ($Å^2$) *for phase* III *at* 295 K

$$B_{eq} = (8\pi^2/3)\sum_i\sum_j U_{ij} a_i^* a_j^* \mathbf{a}_i.\mathbf{a}_j.$$

	Wyckoff position	x	y	z	B_{eq}/B_{iso}
Pb1	8(*g*)	1734 (1)	867 (1)	91 (5)	1.74 (12)
Pb2	8(*g*)	1102 (1)	1741 (1)	5037 (4)	1.21 (11)
Pb3	8(*g*)	1700 (1)	8889 (1)	7 (5)	1.16 (11)
Pb4	8(*g*)	9118 (1)	1722 (1)	4958 (5)	1.40 (11)
Pb5	8(*g*)	9932 (2)	9858 (2)	2352 (9)	3.57 (14)
Al1	2(*c*)	¼	¼	2389 (68)	0.83 (10)†
Al2	2(*c*)	¼	¼	7580 (110)	0.83 (10)†
Al3	4(*f*)	¼	¾	2437 (50)	0.83 (10)†
Al4	8(*g*)	72 (9)	1663 (9)	54 (32)	0.83 (10)†
Al5	8(*g*)	8345 (10)	97 (9)	4921 (29)	0.83 (10)†
F1	2(*c*)	¼	¼	0‡	2.17 (11)†
F2	2(*c*)	¼	¼	½‡	2.17 (11)†
F3	8(*g*)	2150 (15)	1686 (17)	2322 (63)	2.17 (11)†
F4	8(*g*)	2809 (15)	3322 (16)	7553 (69)	2.17 (11)†
F5	2(*a*)	¼	¾	0	2.17 (11)†
F6	8(*g*)	8334 (16)	2171 (16)	2232 (60)	2.17 (11)†
F7	8(*g*)	1669 (16)	7821 (17)	2329 (67)	2.17 (11)†
F8	2(*b*)	¾	¼	½	2.17 (11)†
F9	8(*g*)	695 (18)	1718 (18)	8438 (60)	2.17 (11)†
F10	8(*g*)	9509 (17)	1383 (18)	8415 (55)	2.17 (11)†
F11	8(*g*)	9445 (18)	1475 (19)	1578 (52)	2.17 (11)†
F12	8(*g*)	664 (17)	1931 (18)	1682 (57)	2.17 (11)†
F13	8(*g*)	9883 (16)	2519 (16)	9837 (76)	2.17 (11)†
F14	8(*g*)	307 (19)	820 (18)	434 (51)	2.17 (11)†
F15	8(*g*)	9230 (17)	331 (17)	5062 (71)	2.17 (11)†
F16	8(*g*)	8569 (17)	9462 (17)	3154 (54)	2.17 (11)†
F17	8(*g*)	8428 (17)	9424 (17)	6774 (55)	2.17 (11)†
F18	8(*g*)	8170 (17)	732 (18)	6731 (64)	2.17 (11)†
F19	8(*g*)	8316 (17)	740 (16)	3176 (59)	2.17 (11)†
F20	8(*g*)	7487 (17)	9896 (18)	4546 (71)	2.17 (11)†
F21	8(*g*)	8980 (18)	227 (20)	−96 (63)	2.17 (11)†
F22	8(*g*)	190 (19)	1064 (17)	5122 (70)	2.17 (11)†

† Common variable B_{iso} coefficient for all Al, also for all F, atoms with e.s.d.'s from the least-squares refinement.

‡ Unvaried coordinate.

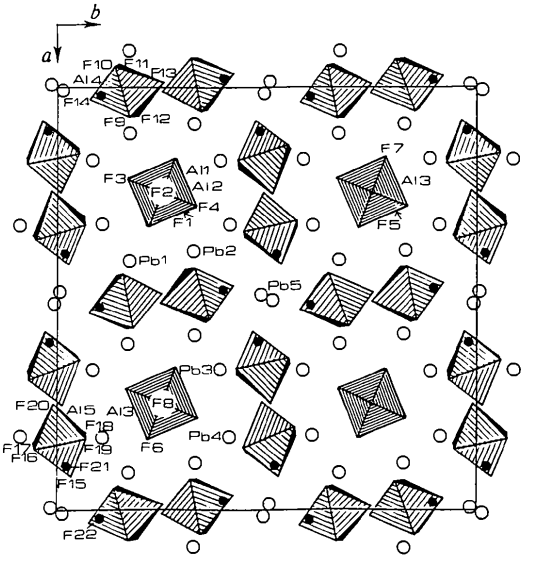

Fig. 1. Projection of the antiferroelectric $Pb_5Al_3F_{19}$ phase III structure along the *c* axis, with AlF_6 octahedra shown shaded. The larger open circles represent Pb and the smaller filled circles the F21 and F22 atoms, see Table 1.

entirely of Al3 F_6 octahedra, above the transition. The remaining independent Al4 F_6 and Al5 F_6 octahedra are oriented approximately normal to the *c* axis. The distribution of the five symmetry-independent Pb^{2+} and two F^- ions is also shown in Fig. 1. The related but reoriented structure of ferroelectric phase IV is shown in Fig. 2. The corner-sharing chains of Al1, Al2 and Al3 octahedra, and also the individual Al4 and Al5 octahedra, are shown in Fig. 3 as viewed along an *a* axis.

$Pb_5Al_3F_{19}$ ferroelectric phase IV

The lattice constants of ferroelectric $Pb_5Al_3F_{19}$ phase IV at 150 K are $a = 14.100$ (3) and $c = 7.344$ (2) Å, whereas those of ferroelectric $Pb_5Cr_3F_{19}$ at 295 K are

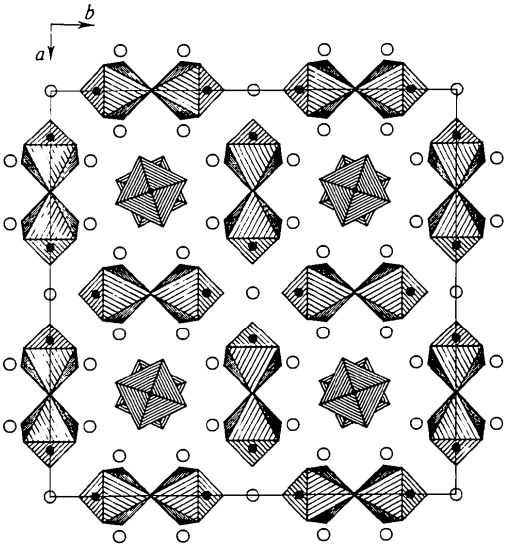

Fig. 2. Projection of the ferroelectric $Pb_5Cr_3F_{19}$ structure along the *c* axis, with axes rotated and the origin translated from the atomic coordinates given by Abrahams *et al.* (1990), as noted in the text, for comparison with Fig. 1.

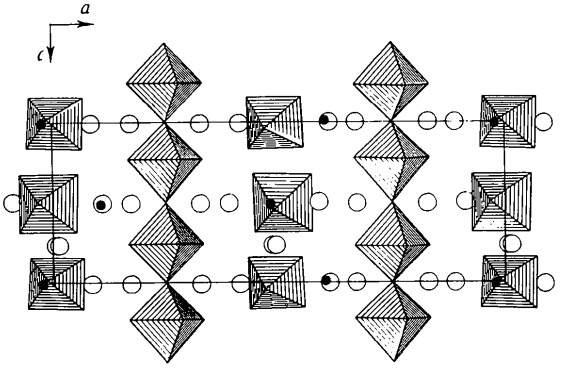

Fig. 3. Projection of the $Pb_5Al_3F_{19}$ phase III structure along an *a* axis, showing the infinite chains both of corner-sharing Al1, Al2 octahedra and corner-sharing Al3 octahedra.

$a = 14.384$ (5) and $c = 7.408$ (2) Å (Arquis-Canouet *et al.*, 1986). The a axes of $Pb_5Al_3F_{19}$, rotated 45° about c in antiferroelectric phase III, increase abruptly in length by about 0.8% to $14.265\sqrt{2}$ Å on heating through the 285 (15) K transition, T_c, while the c axis decreases equally abruptly by about 1.7% to 7.220 (5) Å (Andriamampianina *et al.*, 1991). The close match between the lattice parameters of $Pb_5Cr_3F_{19}$ and $Pb_5Al_3F_{19}$ and the continuous formation of solid solutions of the two materials over the whole composition range (Ravez *et al.*, 1990) strongly suggest that the two are isostructural in their ferroelectric phase. The atomic coordinates of $Pb_5Al_3F_{19}$ in ferroelectric phase IV, stable below 285 K on heating and below 110 K on cooling, may hence be taken as closely comparable to those found in ferroelectric $Pb_5Cr_3F_{19}$ at room temperature.

The transformation of the atomic coordinates (x, y, z) in ferroelectric $Pb_5Cr_3F_{19}$ to a unit cell setting corresponding to that of antiferroelectric $Pb_5Al_3F_{19}$ in phase III requires an origin shift of $\frac{1}{2}$, 0, $\frac{1}{2}$ followed by rotation of the a, b axes through 45°, as given by $x' = (2x + 2y - 1)/4$, $y' = (1 - 2x + 2y)/4$ and $z' = (z - \frac{1}{2})$. The resulting transformed coordinates are shown in Table 2, including the addition of a further translation of 0.04 to all z' coordinates. This additional translation arises from the need to match the arbitrary origin chosen along the polar c axis in ferroelectric phase IV to the fixed origin at the inversion center in antiferroelectric phase III. The atomic numbering in Table 2 corresponds to that in Table 1, with the atomic numbering for the derivative $Pb_5Cr_3F_{19}$ phase at room temperature (Abrahams *et al.*, 1990) given as a subscript. The primes in the transformed $x'y'z'$ coordinates are suppressed in Table 2.

Comparison of the antiferroelectric $Pb_5Al_3F_{19}$ phase III and ferroelectric $Pb_5Cr_3F_{19}$ structures

The atomic arrangement of $Pb_5Al_3F_{19}$ phase III at 295 K determined in the present study is displayed in Fig. 1, that corresponding to the transformed $Pb_5Cr_3F_{19}$ atomic coordinates in Fig. 2. Inspection of Table 2 reveals a total range of differences Δ between the two structures $0.10 \le \Delta \le 1.56$ Å. It may be noted that these differences do not necessarily correspond precisely to the atomic displacements that take place at the transition from the ferroelectric to the nonpolar phase in either $Pb_5M_3F_{19}$ material (M = Cr, Al). Even if the two ferroelectric structures were exactly isostructural, it is unlikely that either coordinate set determined at 295 K would coincide exactly with the actual structures in the thermal regime immediately above or below $T_c(Pb_5Cr_3F_{19})$ or $T_c(Pb_5Al_3F_{19})$. It is to be expected that many values of Δ in either material will be smaller than those listed in Table 2 at temperatures approaching T_c; the largest values listed, however, are likely to remain close to those found at T_c, see *First-order transition from phase IV to phase III*.

Further examination of the differences between corresponding atoms in MF_6 octahedra in the ferroelectric and antiferroelectric phases is revealing. The two symmetry-independent CrF_6 octahedra in ferroelectric $Pb_5Cr_3F_{19}$ at $x = 0$ and $x = \frac{1}{4}$, $y = \frac{1}{4}$ (see Fig. 2) become five independent octahedra in $Pb_5Al_3F_{19}$ phase III. Corner-sharing MF_6 octahedra are located within the unit cells of both phases at $x = \frac{1}{4}$, $y = \frac{1}{4}$ and $x = \frac{1}{4}$, $y = \frac{3}{4}$. In phase III, the Al1 F_6 and Al2 F_6 octahedra on the 4 axis at the former location are fully eclipsed, as are the two Al3 F_6 octahedra on the $\bar{4}$ axis at the latter location. By contrast, in phase IV these octahedra exhibit the staggered configuration clearly visible in Fig. 2. Three independent octahedra in phase III and the corresponding octahedron in phase IV have F—M—F axes parallel to the c axis. These three are now considered in detail. In the case of the $M1_2$–1′ octahedron (see Table 2 for the designation of atoms and symmetry codes), the ferroelectric dipole originating in the displacement of the M atom from the octahedron center is positive in the ferroelectric phase, *i.e.* toward F2. This dipole sense is reversed in the centrosymmetric phase as all atoms in the octahedron are displaced at the transition toward higher z values, with an atomic displacement of about 0.14 Å by the M atom; the dipole is, of course, exactly cancelled within the unit cell by the operation of the inversion centers to form an antiferroelectric array. The major orientational change in this octahedron between the two phases is a rotation of about 48° in the *ab* plane by the group of four F3 atoms.

The $M2_2$–6 octahedron, by contrast, undergoes only a rotation of about 2° in the *ab* plane in the course of the transition between ferroelectric and antiferroelectric phases. The positive dipole moment of this octahedron in the ferroelectric phase, as in the case of the $M1_2$–1′ octahedron, becomes reversed in the centrosymmetric phase. All octahedral and other dipoles are necessarily cancelled in space group $P4/n$ by the inversion-center operation. The $M2_2$–6 octahedron undergoes a translation of about 0.2 Å along the c axis in the transition between the two phases.

The $M3_2$–6′ octahedron similarly has a positive dipole below T_c that becomes reversed in a sense above the phase transition. This octahedron only rotates by about 3° in the *ab* plane as it is translated about 0.1 Å up the c axis. The $M3_2$–1 octahedron, with the M atom at $\frac{1}{4}$, $\frac{3}{4}$, 0.7199 in the ferroelectric phase, rotates about 48° in the *ab* plane at the transition to the antiferroelectric phase; it undergoes a translation of about 0.28 Å at the transition, see Tables 1 and 2.

Table 2. *Atomic coordinates* ($\times 10^4$) *of* $Pb_5Cr_3F_{19}$ *at* 295 K *transformed to the unit-cell setting for* $Pb_5Al_3F_{19}$ *phase* III *and the corresponding atomic displacements* (Å) *between phases* IV *and* III

	Symmetry code*	x	y	z	Δx†	Δy	Δz	Δ
Pb1$_1$‡	5″	1732 (3)	996 (3)	400	0.004	−0.260	−0.223	0.343
Pb2$_1$	1	996 (3)	1732 (3)	5400	0.214	0.018	−0.262	0.343
Pb3$_1$	4′	1732 (3)	9004 (3)	400	−0.065	−0.232	−0.284	0.372
Pb4$_1$	8	9004 (3)	1732 (3)	5400	0.230	−0.020	−0.319	0.394
Pb5$_2$	1′	0	0	1908 (8)	−0.137	−0.286	0.321	0.451
Cr1$_2$	1′	2500	2500	2199 (6)	0	0	0.137	0.137
Cr2$_2$	6	2500	2500	7199 (6)	0	0	0.275	0.275
Cr3$_2$	6′	2500	7500	2199 (6)	0	0	0.172	0.172
Cr4$_1$	7′	0	1632 (6)	293 (12)	0.145	0.063	−0.173	0.234
Cr5$_1$	4	8368 (6)	0	5293 (12)	−0.046	0.196	−0.269	0.336
F1$_7$	5	2500	2500	−277 (71)	0	0	0.200	0.200
F2$_7$	1′	2500	2500	4723 (71)	0	0	0.200	0.200
F3$_3$	6	1639 (14)	2208 (14)	2275 (37)	1.031	−1.053	0.034	1.474
F4$_3$	5‴	3361 (14)	2792 (14)	7275 (37)	1.114	1.069	0.201	1.557
F5$_7$	1	2500	7500	−277 (71)	0	0	0.200	0.200
F6$_3$	4	8361 (14)	2208 (14)	2275 (37)	−0.054	−0.075	−0.031	0.097
F7$_3$	3	1639 (14)	7792 (14)	2275 (37)	0.061	0.059	0.039	0.093
F8$_7$	5	7500	2500	4723 (71)	0	0	0.200	0.200
F9$_1$	2′	714 (16)	1799 (16)	8674 (31)	−0.038	0.163	0.170	0.239
F10$_1$	7′	9286 (16)	1799 (16)	8674 (31)	0.450	−0.839	−0.187	0.970
F11$_2$	2′	9353 (11)	1338 (11)	2055 (16)	0.186	0.276	−0.344	0.479
F12$_2$	7′	647 (11)	1338 (11)	2055 (16)	0.034	1.196	−0.269	1.226
F13$_4$	2′	0	2523 (11)	971 (27)	0.236	0.008	−0.819	0.852
F14$_6$	7′	0	720 (14)	−428 (44)	0.619	0.202	0.622	0.900
F15$_6$	4	9280 (14)	0	4572 (44)	−0.101	0.668	0.354	0.763
F16$_1$	5	8202 (16)	9286 (16)	3674 (31)	0.740	0.355	−0.375	0.902
F17$_2$	4	8663 (11)	9353 (11)	7055 (16)	−0.474	0.143	−0.203	0.535
F18$_2$	5	8663 (11)	647 (11)	7055 (16)	−0.995	0.171	−0.234	1.036
F19$_1$	4	8202 (16)	714 (16)	3674 (31)	0.230	0.052	−0.360	0.430
F20$_1$	4	7477 (11)	0	5971 (27)	0.020	−0.210	−1.029	1.050
F21$_5$	6′	8856 (68)	0	595 (37)	0.250	0.458	−0.499	0.722
F22$_5$	1	0	1144 (8)	5595 (37)	0.383	−0.161	−0.342	0.538

* (1) x, y, z; (2) $-x, -y, z$; (3) $-y, x, z$; (4) $y, -x, z$; (5) $\frac{1}{2}-x, \frac{1}{2}+y, z$; (6) $\frac{1}{2}+x, \frac{1}{2}-y, z$; (7) $\frac{1}{2}+y, \frac{1}{2}+x, z$; (8) $\frac{1}{2}-y, \frac{1}{2}-x, z$. A prime indicates an additional translation of $+(\frac{1}{2},\frac{1}{2},\frac{1}{2})$, a double prime $+(\frac{1}{2},-\frac{1}{2},\frac{1}{2})$, a triple prime $+(0,1,0)$.

† Δx, Δy, Δz are the differences between corresponding atomic coordinates along the a', b', c' axes of the $Pb_5Al_3F_{19}$ and $Pb_5Cr_3F_{19}$ structures, with $\Delta = (\Delta x + \Delta y + \Delta z)^{1/2}$. The lattice parameters of $Pb_5Al_3F_{19}$ are used to calculate the displacements Δ.

‡ Subscript is atom number in ferroelectric $Pb_5Cr_3F_{19}$ structure (Abrahams, Albertsson, Svensson & Ravez, 1990).

The remaining independent octahedra are seen in Figs. 1 and 2 to be rotated, with respect to the $M1$, $M2$ and $M3$ octahedra, by about 45° in the *bc* or *ac* planes. The F13—$M4$—F14 axis in the $M4_1$–7′ octahedron rotates between phases III and IV by about 23° in the *bc* plane and about 14° in the *ab* plane, while the entire octahedron translates along the *c* axis about 0.2 Å. The dipole associated with this octahedron is small below the phase transition, becoming fully cancelled in the antiferroelectric phase as a result of the inversion-center operation. The $M5_1$–4 octahedron undergoes a rotation of about 22° in the *ac* plane and about 14° in the *ab* plane, with a translation along the *c* axis of about 0.3 Å between phases; the intrinsic dipole of this octahedron is small below T_c, with cancellation in the antiferroelectric phase.

First-order transition from phase IV to phase III

The origin of the first-order ferroelectric-to-nonpolar phase transition exhibited by the $Pb_5M_3F_{19}$ materials is clearly associated with the major atomic displacements arising from the MF_6 octahedral rotations and translations. Further experiment is required to determine if the total $M4_1$–7′ and $M5_1$–4 octahedral rotations noted in the previous section of about 25° for each remain as large between the two phases, for a given M atom, as the temperature approaches T_c. The orientation of these two octahedra in the ferroelectric phase could, in principle, move closer to that taken in the antiferroelectric phase as a smooth function of temperature, as would be the case in a second-order phase transition. However, the orientational difference between *staggered* pairs of $M1_2$–1′, $M2_2$–6 and $M3_2$–6′, $M3_2$–1 octahedra along the fourfold rotation axes in the ferroelectric phase and the *eclipsed* orientation of the corresponding pairs found along the inversion- and rotation-tetrad axes in the antiferroelectric phase necessarily persists until the Curie temperature is reached. The thermodynamic barrier associated with an orientational change in these pairs of octahedra as large as that inferred in the present study is entirely consistent with the thermal hysteresis of about 170 K and the coexistence of both phases over about 20 K

reported at the transition in $Pb_5Al_3F_{19}$ from phase III to phase IV on cooling (Ravez *et al.*, 1994).

Interatomic distances in $Pb_5Al_3F_{19}$ phase III at 295 K

The interatomic distances in antiferroelectric $Pb_5Al_3F_{19}$ at room temperature, corresponding to the atomic coordinates in Table 1, are given in Table 3 and may be compared with those found in ferroelectric $Pb_5Cr_3F_{19}$ and elsewhere (Abrahams *et al.*, 1990). The two independent CrF_6 octahedra in $Pb_5Cr_3F_{19}$ at 295 K have average Cr—F distances of 1.922 (25) and 1.851 (9) Å. Standard deviations for all average interatomic distances are calculated from Bessel's formula. The corresponding average Al—F distances in the five symmetry-independent AlF_6 octahedra are 1.795 (51) Å for Al1, 1.782 (36) Å for Al2, 1.806 (39) Å for Al3, 1.750 (30) Å for Al4 and 1.850 (42) Å for Al5; the overall average of 1.796 (39) Å for the Al—F distance in phase III of $Pb_5Al_3F_{19}$ is hence 0.091 Å less than the average of 1.887 Å for the Cr—F distance in ferroelectric $Pb_5Cr_3F_{19}$. The effective ionic radius of Al^{3+} in six coordination as reported by Shannon (1976) is 0.080 Å less than that of Cr^{3+}, in good agreement with the present difference found in ionic radii.

The Pb^{2+} ion forms four nine- and one ten-coordinated F polyhedra in antiferroelectric phase III of $Pb_5Al_3F_{19}$. The range of Pb—F distances is large in each polyhedron, with a minimum of 2.249 (43) Å in the Pb3 F_{10} and a maximum of 3.048 (40) Å in both Pb2 F_9 and Pb4 F_9 polyhedra. The average Pb—F distances are 2.66 (23) Å for nine-coordinated Pb1, 2.72 (23) Å for nine-coordinated Pb2, 2.66 (25) Å for ten-coordinated Pb3, 2.72 (17) Å for nine-coordinated Pb4 and 2.66 (15) Å for nine-coordinated Pb5. The effective ionic radii of 1.49 Å for Pb^{2+} in nine- and 1.54 Å for Pb^{2+} in ten-coordination reported by Shannon (1976), corresponding to Pb—F distances of 2.66 and 2.71 Å, respectively, are fully consistent with the present results. 16 of the 20 independent F atoms in this structure are associated with PbF_n polyhedra, with atoms F1, F2, F5 and F8 not forming Pb—F bonds.

It has been proposed that the sequence of phase transitions in the $Pb_5M_3F_{19}$ materials is strongly influenced by the interaction of the Pb^{2+} ion lone pair of six sp^2 electrons with the $M^{3+}F_6$ octahedra (Ravez *et al.*, 1994). Evidence for the orientation of the lone pair within each of the five symmetry-independent PbF_n polyhedra may be sought by an examination of their distortions. All five PbF_n polyhedra are strongly distorted; Pb1 F_9 may be described as a distorted tricapped trigonal antiprism having F4, F9 and F16 in a lower scalene and F3, F12 and F17 in an upper scalene (along the *c* axis) with F13 and F14 capping faces and F21 capping an edge. The Pb2 F_9 polyhedron may be described as having an upper scalene of F3, F12 and F17 atoms and a lower pair of two F4, F9 and F16 scalenes sharing an F4, F9 edge, with F20 and F22 as capping atoms. Pb3 F_{10} forms a bicapped diagonally compressed cuboid with two F6, two F7, F10, F11, F18 and F19 at the vertices and F13, F21 as capping atoms. Pb4 F_9 may be described as a distorted tricapped trigonal prism formed by the scalenes F6, F7, F20 and F10, F15, F22 with F11 capping a prism face and F18, F19 each capping an edge. The fifth polyhedron, Pb5 F_9, is similarly a distorted tricapped trigonal prism formed by the scalene F10, F14, F16 together with F14 and two F15 atoms; in addition, two F21 atoms and F22 each cap a prism face.

Table 3. *Interatomic distances* (Å) *in* $Pb_5Al_3F_{19}$ *phase III at* 295 K

Al1—F1	1.73 (5)*	Al2—F1^{16}	1.75 (8)
	1.79 (3)		1.77 (6)
—F2	1.89 (5)	—F2	1.86 (8)
Al3—F5	1.76 (4)	Al4—F9^{6}	1.72 (4)
	1.80 (3)	—F11^{19}	1.72 (4)
	1.81 (3)	—F10^{18}	1.74 (4)
—F8^{1}	1.85 (4)	—F12	1.76 (4)
		—F13^{18}	1.78 (4)
Al5—F20^{20}	1.80 (4)	—F14	1.79 (4)
—F19	1.81 (4)		
—F15	1.85 (4)		
—F16^{20}	1.86 (4)		
—F18	1.86 (5)		
—F17^{20}	1.91 (4)		
Pb1—F17^{1}	2.36 (4)	Pb2—F22	2.29 (4)
—F3	2.46 (4)	—F20^{2}	2.53 (4)
—F13^{2}	2.50 (4)	—F9	2.59 (4)
—F16^{3}	2.51 (4)	—F16^{1}	2.84 (4)
—F21^{4}	2.64 (4)	—F17^{1}	2.85 (4)
—F14	2.89 (4)	—F4^{1}	2.85 (4)
—F12^{5}	2.96 (4)	—F3	2.89 (4)
—F9^{6}	2.96 (4)	—F4^{7}	3.05 (4)
Pb3—F21^{3}	2.25 (4)	Pb4—F22^{10}	2.54 (5)
—F19^{3}	2.42 (3)	—F20^{11}	2.54 (4)
—F18^{1}	2.49 (4)	—F11	2.58 (4)
—F13^{8}	2.55 (4)	—F6	2.68 (4)
—F11^{3}	2.68 (4)	—F7^{1}	2.68 (4)
—F6^{3}	2.68 (4)	—F10	2.71 (4)
—F7	2.73 (4)	—F15	2.82 (4)
—F10^{1}	2.75 (4)	—F19	2.86 (4)
—F6^{5}	3.00 (4)	—F18	3.05 (4)
—F7^{9}	3.04 (4)		
Pb5—F14^{3}	2.48 (4)	Pb5—F21^{13}	2.71 (4)
—F14^{12}	2.50 (4)	—F21^{15}	2.74 (4)
—F15^{14}	2.55 (5)	—F10^{14}	2.80 (4)
—F15^{13}	2.60 (5)	—F16	2.92 (4)
—F22^{1}	2.62 (5)		

* Symmetry codes for Table 3: (1) $1-x, 1-y, 1-z$; (2) $\frac{1}{2}-y, -1+x, -1+z$; (3) $1-x, 1-y, -z$; (4) $1-x, -y, -z$; (5) $\frac{1}{2}-y, x, z$; (6) $x, y, -1+z$; (7) $1-y, -\frac{1}{2}+x, 1-z$; (8) $\frac{1}{2}-y, x, -1+z$; (9) $-\frac{1}{2}+y, 1-x, -z$; (10) $1+x, y, z$; (11) $2-y, -\frac{1}{2}+x, 1-z$; (12) $1+x, 1+y, z$; (13) $x, 1+y, z$; (14) $2-x, 1-y, 1-z$; (15) $2-x, 1-y, -z$; (16) $x, y, 1+z$; (17) $y, \frac{3}{2}-x, z$; (18) $-1+x, y, -1+z$; (19) $-1+x, y, z$; (20) $x, -1+y, z$; (21) $\frac{1}{2}-x, \frac{1}{2}-y, z$; (22) $\frac{1}{2}-x, \frac{1}{2}-y, z-1$.

It may be noted that the only polyhedra in phase III similar in shape to those reported in phase IV are Pb4 F_9 and Pb5 F_9; these are also the only two polyhedra with all Pb—F distances greater than about 2.5 Å. The three other polyhedra each have one short Pb—F distance, 2.36 (4) Å for Pb1, 2.29 (4) Å for Pb2 and 2.25 (4) Å for Pb3. Bond overlap with the lone pair is expected to reduce the Pb—F distance. It may also be noted that the short Pb—F distances in the Pb2 and Pb3 polyhedra are directed toward capping atoms. Direct determination by X-ray diffraction of the lone-pair orientation in these Pb compounds requires a structure-factor accuracy no less than about 1%, an achievement that will become possible with the growth of larger and higher quality crystals. Investigation of the $Pb_5Al_3F_{19}$ structure in the remaining phases, now in progress, may contribute further to understanding the rôle of the Pb lone pair.

References

ABRAHAMS, S. C., ALBERTSSON, J., SVENSSON, C. & RAVEZ, J. (1990). *Acta Cryst.* B**46**, 497–502.

ABRAHAMS, S. C., KURTZ, S. K. & JAMIESON, P. B. (1968). *Phys. Rev.* **172**, 551–553.

ANDRIAMAMPIANINA, V., RAVEZ, J., SIMON, A. & ABRAHAMS, S. C. (1991). *Phase Transit.* **33**, 77–79.

ARQUIS-CANOUET, S., RAVEZ, J. & ABRAHAMS, S. C. (1986). *J. Appl. Cryst.* **19**, 374–376.

IHRINGER, J., RAVEZ, J. & ABRAHAMS, S. C. (1993). *Zeit. Kristallogr.* In the press.

RAVEZ, J., ANDRIAMAMPIANINA, V., SIMON, A., GRANNEC, J. & ABRAHAMS, S. C. (1991). *J. Appl. Phys.* **70**, 1331–1336.

RAVEZ, J., ANDRIAMAMPIANINA, V., SIMON, A., RABARDEL, L., IHRINGER, J. & ABRAHAMS, S. C. (1994). *J. Appl. Cryst.* In the press.

RAVEZ, J., SIMON, A., ANDRIAMAMPIANINA, V., GRANNEC, J., HAGENMULLER, P. & ABRAHAMS, S. C. (1990). *J. Appl. Phys.* **68**, 3529–3531.

SHANNON, R. D. (1976). *Acta Cryst.* A**32**, 751–767.

SHELDRICK, G. M. (1976). *SHELX76. Program for Crystal Structure Determination.* Univ. of Cambridge, England.

Acta Cryst. (1994). B**50**, 141–146

Space Group of the Trirutile Type Structure of Li_2MoF_6

BY WERNER H. BAUR

Institut für Kristallographie und Mineralogie, Senckenberganlage 30, *D*-60054 *Frankfurt am Main, Germany*

(*Received* 2 *August* 1993; *accepted* 27 *October* 1993)

Abstract

Dilithium molybdenum hexafluoride, Li_2MoF_6, tetragonal, $M_r = 223.83$, $a = 4.6863$ (7), $c = 9.191$ (2) Å, $V = 201.8$ (2) Å^3, $D_x = 3.683$ Mg m^{-3}, λ(Mo $K\alpha$) = 0.71069 Å, $F(000) = 206$, single crystal refinement to $R = 0.057$ in space group $P4_2/m2_1/n2/m$ based on 371 structure factors measured on a diffractometer by Brunton [(1971). *Mater. Res. Bull.* **6**, 555] who preferred in his refinement of the same data space group $P4_22_12$. Refinements in space groups $P4_2$, $P4_22_12$ and $P4_2/m2_1/n2/m$ show that Li_2MoF_6 crystallizes in the most highly symmetric of these space groups and is, therefore, isostructural with the aristotypic trirutile type. The decision for space group $P4_2/m2_1/n2/m$ is based on the shape and orientation of the displacement ellipsoid of the F(1) atom and on the extremely high R value of the reflections not obeying the extinction condition of the n glide in space group $P4_22_12$. The importance of the weak reflections in deciding a centrosymmetric–non-centrosymmetric space-group ambiguity is emphasized.

Introduction

The crystal structure of rutile, one of the three naturally occurring polymorphs of TiO_2, was determined by Vegard (1916). Goldschmidt (1926) determined the crystal structures of the minerals mossite, $Fe(Nb,Ta)_2O_6$, and tapiolite, $FeTa_2O_6$. They crystallize in a superstructure of the rutile type, which could be derived by a tripling of the c cell constant. The space group type was the same as for rutile, $P4_2/m2_1/n2/m$, and the cations were distributed in an ordered way over the octahedrally coordinated cation positions, thus generating the superstructure. Goldschmidt (1926) coined the term trirutile for this arrangement. This structure type has been identified in a variety of oxides and fluorides, in which mostly two different octahedrally coordinated cations occur in a ratio of 2:1 (AB_2X_6). The trirutile type is best defined narrowly as a derivative of rutile, with a tripled c cell constant and space group $P4_2/m2_1/n2/m$ (Baur, 1994). In the case of this space group, the maximal isomorphic *klassengleich* subgroup of the lowest index is of

©1994 International Union of Crystallography
Printed in Great Britain – all rights reserved